https://doi.org/10.1016/j.enconman.2018.10.044

Thermodynamic and economic investigation of a humidification dehumidification desalination system driven by low grade waste heat

Weifeng He*[1], Hongxing Yang[1], Tao Wen[1], Dong Han[2]

1. Renewable Energy Research Group (RERG), Department of Building and Services Engineering, The Hong Kong Polytechnic University, Hong Kong, China

2. Nanjing University of Aeronautics and Astronautics, College of Energy and Power Engineering, Nanjing, 210016, China

Corresponding author: W.F. He

The Hong Kong Polytechnic University

Hung Hom, Kowloon, Hong Kong

Tel./Fax numbers: +852 27665863

E-mail address: wfenghe@polyu.edu.hk, wfhe@nuaa.edu.cn

ABSTRACT: This paper focuses on the thermodynamic and economic investigation of a humidification dehumidification desalination system (HDDS), using waste exhaust gas to heat the humid air. In accordance with the principles of the mass and energy conservation, thermodynamic analysis of the HDDS is first completed, and the heat and mass transfer (HMT) areas for the waste heat recovery exchanger, packing-bed humidifier and plate type dehumidifier, are obtained. Finally, the economic performance of the HDDS is also calculated. The research results state clearly that the top values of the water production and GOR arrive at 289.32kgh^{-1} and 3.06 at the dehumidification balance conditions, while the maximum total investment of the air-heated HDDS is calculated as 112.55×10^{3}¥. The influence laws from the variation of the dehumidification effectiveness, minimum enthalpy difference during humidification, top temperature and temperature of the waste heat source are different and complicated, especially on the unit cost of water production, which is determined with the thermodynamic and economic performance considered simultaneously. It can be concluded that the elevation of the thermodynamic

performance, mainly referring to the aspect of water production, will raise the corresponding cost of the air-heated HDDS, which is mainly composed of the investment of the dehumidifier area.

Keywords: humidification dehumidification desalination system; waste exhaust gas; thermodynamic analysis; heat and mass transfer; economic performance

Nomenclature

Roman symbols	
A	heat transfer area (m^2)
b	channel height of the plate (mm)
h	convective heat transfer coefficient (Wm^2K^{-1})
i	enthalpy ($kJkg^{-1}$)
I	total enthalpy (kW)
K	overall coefficient ($Wm^{-2}K^{-1}$)
m	mass flow rate (kgs^{-1})
Nu	Nusselt number
Q	heat load (kW)
P_r	Prandtl number
Re	Reynolds number
S	seawater concentration (gkg^{-1})
ΔT	temperature difference (K)
T	temperature (K)
v	velocity (ms^{-1})
V	packing volume (m^3)
W	plate width (m); power (kW)
Greek letters	
β	plate chevron angle (°)
ψ	minimum enthalpy difference ($kJkg^{-1}$)
δ	plate thickness (mm)
ρ	density (kgm^{-3})
μ	dynamic viscosity($kgm^{-1}s^{-1}$)
ε	effectiveness
ω	absolute humidity (gkg^{-1})
Subscripts	
a	air; ambient
b	brine; blower
d	dehumidifier
da	dry air
e	exhaust
h	humidifier

i	inlet
o	outlet
p	plate
pu	pump
sw	seawater
w	water; wet
WHRE	waste heat recovery exchanger

1. Introduction

In view of the uniform distribution of freshwater and serious pollution, water supply has been a universal problem. Different desalination methods, mainly including thermal [1, 2] and membrane prototype [3, 4], were proposed constantly, to provide water from seawater or brackish water. For such desalination systems, huge amount of energy was consumed and the corresponding configurations were complicated [5]. Consequently, the economic performance of the complicated systems was confined. Furthermore, due to the trend of extensive utilization for renewable energy, the potential applications of the desalination systems, with huge energy consumption and complicated configurations, are not very prospective, especially for the demands for small scale of water.

As a result, desalination systems with higher thermal efficiency and lower cost is in demand to supply freshwater. Recent years, the humidification dehumidification desalination prototypes, which simulated the water circulation in the nature, were proved to be promising, and they were extensively investigated all over the world [6, 7]. A water-heated HDDS, driven by solar radiation at the seawater aspect, was proposed by Hamed et al. [8], and theoretical models for the components were built to assess the thermodynamic performance. Two periods with different solar radiations were selected to investigate the water producing capacity of the HDDS. The simulation results presented the best water producing capacity was found during the second period, from 13 to 17 pm. In addition of the simulation research, the experimental platform was also established to validate the HMT characteristics involved in the desalination process, and the mathematical models were proved to be accuracy with a good consistency between the calculation results and test data under different boundary conditions. Al-Sulaiman et al. [9] introduced a solar collector with parabolic trough into an open air and open water air-heated HDDS.

Thermodynamic performance of the HDDS was focused, and influence mechanism on the system performance from the solar heater configurations were found. It was found that the solar driven air-heated HDDSs were suitable for the locations with high radiation. A semi-open air and open water configuration of the HDDS was proposed to produce water by Mahdizade and Ameri [10]. The prototype, with heating air and water at the same, was proved to be effective for raising the water producing capacity.

Narayan et al. [11] and Chehayeb et al. [12] suggested a modified definition of effectiveness for the HMT processes, overcoming the problems from the fixed model of effectiveness [13, 14]. Chehayeb et al. [15] achieved the thermodynamic balancing for single and two-stage water-heated HDDS, with a humidifier filled by packings and a bubble column dehumidifier. The laws of the flow rate ratio to influence the system entropy generation and forces of HMT processes were revealed. Based on the modified definition of energy effectiveness, the air extraction and injection were applied to enhance the performance of the HDDS, and the improvement effect and relevant mechanism were investigated.

It can be concluded that the thermodynamic performance of the HDDS, including the water-heated and air-heated configurations, was studied extensively. However, taking the potential applications into consideration, the relevant economic aspect should also be the important research objective [16]. Deniz and Cinar [17] and Zubair et al. [18] established the economic models of the water-heated HDDS driven by solar energy. The thermodynamic performance, including the water producing capacity and thermal efficiency, were first calculated and assessed at different solar radiations, and the corresponding cost of the entire system was also obtained. Jamil et al. [19] obtained the exergo-economic performance of the HDDS, with two different configuration, and a reverse osmosis system was also coupled to the HDDS. The research results presented that the modified configuration had advantages both in the exergetic efficiency and system cost. It was also found that that the hybrid system, with HDDS and reverse osmosis subsystem integrated, had a highest gained output ratio and second-law efficiency.

Lawal et al. [20] investigated the exergo-economic performance of the HDDS powered by a heat pump with vapor compression, with three different integration prototypes. Exergetic efficiency, exergy destruction and cost of the entire system were calculated, and the impact laws from the critical thermal parameters on the system performance were analyzed. The results showed the evaporator and compressor had the largest exergy destruction, and the air-heated HDDS driven by heat pump was suggested to be applied due to the better performance at the viewpoints of energetic and exergetic.

From the literature survey, it can be obtained that the economic analysis of the HDDS, mainly referring to the water-heated configuration, has been focused. However, it was proved that the air-heated prototype had obvious advantages with a higher gained-output-ratio, compared to the water-heated one [10]. Thus, the economic analysis of the conventional air-heated HDDS must be studied to explore the application potential, while it was not the research focus previously. Furthermore, the modified model of effectiveness simulating the humidification process was applied into the water-heated HDDS, while such application was not achieved in the air-heated type. In this paper, the aspects of air-heated HDDS, modified definition of effectiveness and economic analysis were first integrated together. Thermodynamic performance of the integrated desalination system was simulated in accordance with the established mathematical models. Afterwards, the corresponding economic performance was also obtained based on the simulated thermal parameters. Furthermore, influence laws of the dehumidification effectiveness, minimum enthalpy difference during humidification, air top temperature and the temperature of the waste heat source on the system performance are also obtained. The built mathematical models and simulation results provide significant guidance for the design and optimization of the HDDS.

2. System description of the air-heated HDDS

As known, the air-heated HDDS is comprised of a packed bed humidifier, plate type dehumidifier and waste heat recovery exchanger, with a open water, closed air configuration, presented in Fig. 1. It can be found that in the

packed bed humidifier, hot seawater, which is heated by the hot humid air, is sprayed into the filled packings. As a result, the hot seawater is concentrated while the air is humidified. Afterwards, the humid air is further heated in the waste heat recovery exchanger through the waste exhaust recovery. Finally, the carried steam by the hot humid air is removed under the cooling effect of the feed seawater, and water is produced, flowing out of the dehumidifier bottom. The dehumidified air enters the humidification process again to close the air cycle.

The situations of the energy conversion and heat transfer processes are described and shown in the T-h diagram [12], with curves described by different colors in Fig. 2, which is composed of the humidification, dehumidification and waste heat recovery. It can be summarized that the produced water is mainly resulted from the difference of the absolute humidity, and the energy input into the humid air is recovered by the seawater during dehumidification. The preheated seawater is used to raise the temperature and absolute humidity of the air. Consequently, the input energy can be reduced to improve the energy conversion within the air-heated HDDS.

To model the air-heated HDDS and achieve the performance analysis, the following assumptions are given out:

(1) The air-heated HDDS operates at the steady-state conditions.

(2) Kinetic and potential energy variations, energy loss to the surroundings during all the thermal processes are ignored.

(3) Foulings are neglected during simulating the characteristics during heat transfer.

(4) Pressure drops within the pipes is not considered during assessing the power consumption of the blowers and pumps. Furthermore, it is assumed that the spraying pressure is three times the ambient pressure, p_a.

3. Thermodynamic models of the air-heated HDDS

3.1 Waste heat recovery exchanger

A plate heat exchanger is used to achieve the waste heat recovery, raising the air temperature from the outlet of the humidifier. Hence, the heat balance within the heat exchanger is expressed in Eq. (1).

$$Q_{WHRE} = \mathrm{m_e}(i_{e,i} - i_{e,o}) = m_{da}(i_{a3} - i_{a2}) \tag{1}$$

Furthermore, during the heat process of the humid air, the absolute humidity keeps the same in Eq. (2).

$$\omega_2 = \omega_3 \tag{2}$$

In order to complete the thermodynamic and economic analysis, heat transfer area of the WHRE should be calculated, and the heat transfer coefficients both of the waste exhaust and humid air aspect should be obtained. For a plate type heat exchanger, Muley and Manglik [21] gave out the specific function of the Nusselt number, with plate chevron angle, β, area expansion coefficient, φ, Reynolds number, *Re*, and Prandtl number, *Pr*, as the independent variables, and the specific dimensions of the involved plate heat exchangers are listed in Table 1.

$$\begin{aligned} Nu = {} & (0.2668 - 0.006967\beta + 7.244\times10^{-5}\beta^2)(20.78 - 50.94\varphi + 41.16\varphi^2 - 10.15\varphi^3) \\ & \mathrm{Re}^{(0.728+0.0543\sin(\pi\beta/45+3.7))}\,\mathrm{Pr}^{1/3}(\mu/\mu_w)^{0.14} \end{aligned} \tag{3}$$

Hence, the convective coefficients of the waste exhaust and air aspects as well as the total heat transfer coefficient, *K*, can be calculated, and the heat transfer area for recovering the waste heat can be calculated in Eq. (4).

$$A_{WHRE} = \frac{Q_{WHRE}}{K\Delta T_{WHRE}} \tag{4}$$

Furthermore, the air pressure loss through the waste heat recovery exchanger can be obtained from the following expression [21].

$$\begin{cases} f = (2.917 - 0.1277\beta + 2.016\times10^{-3}\beta^2)(5.474 - 19.02\varphi + 18.93\varphi^2 - 5.341\varphi^3) \\ \qquad \mathrm{Re}^{-(0.2+0.0577\sin(\pi\beta/45+2.1))} \\ \Delta p = 2f\dfrac{L}{D_h}(\rho v^2)(\mu/\mu_w)^{-0.17} \end{cases} \tag{5}$$

3.2 Humidifier

In the humidifier, the dehumidified air contact the sprayed seawater. After the HMT process, mass and energy balance will arrive as the following equations:

$$m_{sw} - m_b = m_{da}(\omega_2 - \omega_1) \tag{6}$$

$$m_{sw} i_{sw,1} - m_b i_b = m_{da}(i_{a2} - i_{a1}) \tag{7}$$

During simulating the performance of the HDDS, the HMT characteristics of the humidification has great significance. In this paper, a modified definition of effectiveness, ε_h [12], is applied to determine the specific parameters, expressed in Eq. (8).

$$\varepsilon_h = \frac{\Delta i}{\Delta i + \psi_h} \tag{8}$$

After the inlet and outlet parameters during humidification are determined from the mass and energy conservation, the characteristics of the mass transfer process, including the packing volume, V_h, and mass transfer coefficient, k_h, are attained [22]:

$$m_{da}(i_{a2} - i_{a1}) = k_h a_p V_h \left[\frac{(i_{sw,1s} - i_{a2}) - (i_{b,s} - i_{a1})}{\log\left(\frac{i_{sw,1s} - i_{a2}}{i_{b,s} - i_{a1}}\right)}\right] \tag{9}$$

$$\frac{k_h a_p V_h}{m_{sw} / \left(\frac{\pi}{4} d_h^{\,2}\right)} = (1.222 H_h + 0.367)\left(\frac{m_{sw}}{m_{da}}\right)^{(-0.66)} \tag{10}$$

With respect to the air flow loss through the packings, it can be calculated according to the models from Gandhidasan [23].

3.3 Dehumidifier

After the humidification and heating process in the WHRE, the heated humid air enters the dehumidifier, which is also a plate type heat exchanger essentially, and the carried is removed as the produced water under the cooling effect of the feed seawater. According to the mass and energy conservation, the corresponding balance equations can be expressed as:

$$m_w = m_{da}(\omega_3 - \omega_1) \tag{11}$$

$$m_{sw}(i_{sw,1} - i_0) + m_w i_w = m_{da}(i_{a3} - i_{a1}) \tag{12}$$

For the plate type dehumidifier, the characteristics are described by the fixed effectiveness model, which can be defined as:

$$\begin{cases} \varepsilon_d = \dfrac{\Delta I}{\Delta I_{\max}} \\ \Delta I_{\max} = \min(\Delta I_{\max,sw}, \Delta I_{\max,air}) \end{cases} \tag{13}$$

In order to complete the thermodynamic and economic analysis, heat transfer area of the WHRE should be calculated, and the heat transfer coefficients both of the waste exhaust and humid air aspect should be obtained. For a plate type heat exchanger, Muley and Manglik [21] gave out the specific function of the Nusselt number, with plate chevron angle, β, area expansion coefficient, φ, Reynolds number, *Re*, and Prandtl number, *Pr*, as the independent variables, and the specific dimensions of the involved plate heat exchangers are listed in Table 1.

$$\begin{aligned} Nu = {} & (0.2668 - 0.006967\beta + 7.244\times10^{-5}\beta^2)(20.78 - 50.94\varphi + 41.16\varphi^2 - 10.15\varphi^3) \\ & \mathrm{Re}^{(0.728+0.0543\sin(\pi\beta/45+3.7))}\,\mathrm{Pr}^{1/3}(\mu/\mu_w)^{0.14} \end{aligned} \tag{3}$$

Hence, the convective coefficients of the waste exhaust and air aspects as well as the total heat transfer coefficient, *K*, can be calculated, and the heat transfer area for recovering the waste heat can be calculated in Eq. (4).

$$A_{WHRE} = \frac{Q_{WHRE}}{K\Delta T_{WHRE}} \tag{4}$$

Furthermore, the air pressure loss through the waste heat recovery exchanger can be obtained from the following expression [21].

$$\begin{cases} f = (2.917 - 0.1277\beta + 2.016\times10^{-3}\beta^2)(5.474 - 19.02\varphi + 18.93\varphi^2 - 5.341\varphi^3) \\ \qquad \mathrm{Re}^{-(0.2+0.0577\sin(\pi\beta/45+2.1))} \\ \Delta p = 2f\dfrac{L}{D_h}(\rho v^2)(\mu/\mu_w)^{-0.17} \end{cases} \tag{5}$$

169

170 Furthermore, at the aspect of the heat transfer characteristics, the convective heat transfer coefficient of the air

171 without condensation, h_d, can be calculated according to Eq. (3), and the corresponding value at wet conditions, h_w,

172 can be updated with the following relation [24]:

173 $$h_w = h_d(0.164\ln(\mathrm{Re}) - 0.02) \tag{14}$$

174 With respect to the pressure drop within the dehumidifier, the relevant values both for the seawater and air

175 aspects can be obtained based on the principles demonstrated in Eq. (5).

176 **3.4 Blower**

177 For air-heated HDDS, the power consumption of the blower, W_b, should be considered, and it can be

178 calculated based on the air mass flow rate and the flow losses within the HMT devices, in Eq. (11), with a blower

179 efficiency of η_b=0.8.

180 $$W_b = \frac{m_a}{\rho_a \eta_b}(\Delta p_{WHRE} + \Delta p_h + \Delta p_{d,a}) \tag{15}$$

181 **3.5 Pump**

182 The consumed power of the pump can be calculated based on the seawater mass flow rate and the relevant

183 flow loss, and the relevant value can be obtained as follows, with an efficiency of η_{pu}=0.8:

184 $$W_{pu} = \frac{m_{sw}}{\rho_{sw}\eta_{pu}}(\Delta p_{d,sw} + 3p_a) \tag{16}$$

185 **3.6 Performance of the air-heated HDDS**

186 For a desalination system, gained-output-ratio (GOR) is usually used to characterize the energy conversion

187 efficiency. With the water production and different energy consumptions into consideration, the gained-output-ratio

188 can be calculated in Eq. (17), in which the power consumption is converted to the equivalent thermal energy during

189 power generation with η_e=40% [25].

$$GOR = \frac{m_w i_{fg}}{Q_{WHRE} + (W_b + W_{pu}) / \eta_e} \tag{17}$$

4. Economic models of the air-heated HDDS

After the thermodynamic analysis based on the previous mathematical models, the scales of the devices within the HDDS can be fixed. Hence, in combination with the material and type of the devices, shown in Table 2, the capital costs of the plate type heat exchangers, packings, pump and blower can be obtained with the following equation:

$$C_t = C_{WHRE} + C_{\mathrm{d}} + C_h + C_{\mathrm{b}} + C_{pu} \tag{18}$$

where C_{WHRE}, C_d, C_h, C_b and C_{pu} are the cost of the WHRE, dehumidifier, humidifier, blower and pump. Furthermore, the definition, unit cost of water production (UCWP), is also used to characterize the cost for producing 1kg freshwater in Eq. (19).

$$UCWP = \frac{C_t}{3600 m_w} \tag{19}$$

5. Validation of the thermodynamic models

In order to affirm the reliability of the mathematical models for the air-heated HDDS, the accuracy of the humidification and dehumidification performance is compared to the published results under the same input conditions. The obtained temperature profile along the non-dimensional location, at ψ_h=20kJkg^{-1}, is first compared to that from Chehayeb et al. [12] in Fig. 3, and the maximum deviation emerges as 0.65% for the seawater temperature at the outlet of the humidifier. Furthermore, the dehumidification performance is also compared with the classical published data from Narayan et al. [26] in Table 3, and a peak deviation of the producing water, 5.1%, is obtained. Hence, the comparison results of the humidification and dehumidification performance, between the investigated system and that from the references, verify the reliability of the proposed mathematical models.

5. Results and discussion

In the current investigation, thermodynamic performance of the air-heated HDDS is first simulated, on the basis of the design parameters shown in Table 4, and then the change laws of the economic performance are also calculated with the critical parameters, including the effectiveness of the dehumidifier, minimum enthalpy difference during humidification and the top air temperature after the waste heat recovery process. During the simulation, the properties of the waste exhaust can be found in Table 5, and the research strategy and specific procedures in the Matlab platform are presented in Fig. 4, with the previous conservation equations solved iteratively.

5.1 Thermodynamic performance of the air-heated HDDS at design conditions

Based on the design conditions shown in Table 4, the water production within the air-heated HDDS is simulated and presented in Fig. 5(a), including the water production and the gained-output-ratio. As demonstrated by Chehayeb et al. [12], due to a minimum specific entropy generation rate at the dehumidification balance conditions, a best performance of the HDDS can be obtained. In the current situation, the maximum water production emerges as m_w=289.32kgh^{-1} when the mass flow rate ratio between the seawater and dry air stays at m_{sw}/m_{da}=0.95. Actually, the variation laws of the water production with the mass flow rate ratio are mainly attributed to the trend of the air humidity difference before and after dehumidification. It can be observed that the humidity difference of the humid air arrives at $\Delta\omega$=47.38gkg^{-1}, which is a peak value within the range of the mass flow rate ratio from m_{sw}/m_{da}=1 to m_{sw}/m_{da}=3.6. It is also seen that the water producing capacity will be restrain with the increase of the mass flow rate ratio. At the fixed top temperature of the humid air and dehumidification, with T_{a3}=353.15K and ε_d=0.85, the discharge temperatures both for the seawater and humid air at the dehumidifier outlet will decrease continuously, which also confines the effective mass flow rate ratio. As a result, the maximum mass flow rate ratio stays at m_{sw}/m_{da}=3.6, and the relevant temperatures of the seawater and humid air at the outlet are $T_{sw,1}$=306.70K and T_{a1}=304.95K. Evidently, the temperature difference between the seawater and humid air

indicates the driving force during the mass transfer process in the humidification. A very limited temperature difference, between the values of $T_{sw,1}$ and T_{a1}, results in a humidity difference of $\Delta\omega$=0.11gkg^{-1} and a water production of m_w=0.60kgh^{-1}.

At the aspect of the thermal efficiency during water production, GOR, the corresponding variation laws are also presented in Fig. 5(b). It is found that a maximum value, *GOR*=3.06, is found at the dehumidification balance conditions. It is illustrated that the input energy to the HDDS mainly contains the recovered energy from the exhaust gas, the power consumed by the seawater pump and blower. Taking the dehumidification balance conditions into consideration, the relevant values of the recovered energy and the power consumption are Q_{WHRE}=60.02kW, W_{pu}=0.62kW for the seawater pump and W_b=0.20kW for the blower, respectively. It can be concluded that the recovered energy has the dominant weight within the entire range of the mass flow rate ratio, although the variation laws of the energy consumption from three paths are different. In fact, the temperature of humid air at after humidification, T_{a2}, reaches the peak value, T_{a2}=322.77K, at the dehumidification balance conditions, and a corresponding bottom value for the recovered energy, Q_{WHRE}=60.02kW, is obtained. In combination with the trend of the water production, the best energy conversion situation is gained, with a peak value, *GOR*=3.06, for the definition of GOR.

The thermodynamic results of the HDDS can be compared to those from the same system, using the general definition of effectiveness to describe the performance both for humidification and dehumidification [27]. It can be found that the actual top value of GOR arrived at *GOR*=3.04, when the effectiveness both for humidifier and dehumidifier were fixed at ε=0.9. It can be concluded that the peak energy conversion efficiencies of the air-heated HDDS are equivalent under the conditions with the current design conditions, ψ_h=10kJkg^{-1} and ε_d=0.9, and that from [27].

5.2 Cost of the air-heated HDDS at design conditions

According to the obtained thermal parameters from the performance simulation, the dimensions of HMT devices, including the humidifier, dehumidifier and WHRE, can be calculated, shown in Fig. 6(a). Corresponding to the best performance at the dehumidification balance conditions for the air-heated HDDS, a top heat transfer area of the dehumidifier, A_d=197.78m^2, is attained, because the heat load of the dehumidifier is proportional to the water production. Moreover, a bottom heat transfer area for the WHRE, A_{WHRE}=55.78m^2, is also obtained mainly resulting from the change laws of the relevant heat load with the increasing mass flow rate ratio. With respect to the situation of the packings, a minimum volume as V_h=0.06m^3 appears, because the superficial velocity through the packings reaches the peak value, which also indicates a peak power of the blower, W_b=1.8kW, shown in Fig. 5(b). As demonstrated previously, the performance of the air-heated HDDS will be affected seriously, when the mass flow rate ratio rises. For the component of the humidifier, to realize the fixed enthalpy difference as ψ_h=10kJkg^{-1}, the dehumidifier with a larger volume must be applied to compensate the lower performance during the mass transfer process. For example, the packing volume arrives at V_h=9.89m^3, while the relevant effectiveness, ε_h, is only ε_h=0.03 according to Eq. (8).

After the HMT areas are obtained, the relevant component cost, shown in Fig. 6(b), is also calculated in view of the properties of the involved materials in Table 2. Obviously, the change laws of the cost for the HMT devices are similar with those of the relevant areas in Fig. 6(a). A peak cost of the dehumidifier arises with C_d=104.30×10^3¥. Moreover, the cost of the power machinery, is also obtained according to the listed information of the pump and blower in Table 6. Three types of the pumps are selected in accordance with the power scale, while the only type of the blower is applied. Finally, total investment of the air-heated HDDS can be acquired, with the cost of all the contained devices accumulated, and the relevant value is C_t=112.55×10^3¥ at the dehumidification balance conditions.

5.3 Effects from the effectiveness of the dehumidifier

In the air-heated HDDS, the water is produced during the condensation of the hot humid air in the dehumidifier, and the dehumidification characteristics are important for the performance of the entire system. As a result, different values with 0.8, 0.85 and 0.9, are prescribed to investigate the influence laws from the dehumidification effectiveness on the thermodynamic and economic performance of the HDDS, shown in Fig. 7. In response to the alternation of the dehumidification effectiveness, from ε_d=0.8 to ε_d=0.9, it can be found that the peak water production rises from m_w=236.47kgh^{-1} to m_w=362.22kgh^{-1}, with an elevation magnitude of 53.18%, at the dehumidification balance conditions. In light of the relation between the water production and the thermal efficiency, the value of GOR increases from *GOR*=2.45 to *GOR*=3.94 spontaneously.

It has been proved that the higher the values of the water production and GOR are, the more expensive the air-heated HDDS is. Taking the simulation results from the design conditions for instance, the highest values, m_w=289.32kgh^{-1} for the water production, and C_t=112.55×10^3¥ for the total cost exist simultaneously, at the dehumidification balance conditions. In combination with the cost distribution of all the devices presented in Fig. 7(b), it is calculated the top cost of the entire HDDS is increased sharply from C_t=52.46×10^3¥ at ε_d=0.8 to C_t=431.75×10^3¥ at ε_d=0.9. Consequently, an elevation amplitude, Δm_w=125.75kgh^{-1}, for the water production will contribute to a jump, ΔC_t=379.29×10^3¥, for the total cost of the desalination system, which is mainly attributed to the increase of the area for the dehumidifier, from A_d=83.64m^2 to A_d=803.42m^2.

Furthermore, in order to characterize the unit cost to achieve water production, UCWP is defined as the total cost divided by the water production. Regardless of the conditions with high mass flow rate ratio, which stands for very low humidification effectiveness, a top value of UCWP is also discovered at the dehumidification balance conditions, and it is raised from *UCWP* =0.22×10^3¥kg^{-1}h at ε_d=0.8 to *UCWP* =1.19×10^3¥kg^{-1}h at ε_d=0.9.

5.4 Effect from the minimum enthalpy difference of the humidifier

In addition of the dehumidifier, the humidifier with filled packings is also the core device, which produces the

hot humid air to be condensed during dehumidification. Thus, the relevant water producing capacity, which can be represented by the humidification effectiveness in some extent, is also important for the thermodynamic and economic performance of the entire HDDS. In this paper, the modified definition of effectiveness for the heat and mass exchangers [12] is applied, which can be calculated through the minimum enthalpy difference, ψ_h. Accordingly, three different enthalpy differences, with 5kJkg^{-1}, 10kJkg^{-1} and 15kJkg^{-1}, are appointed to study the influences from the humidification performance on the performance of the entire HDDS, exhibited in Fig. 8.

The definition equation, Eq. (8), is used to calculate the humidification effectiveness. It is obvious that a lower enthalpy difference indicates a higher effectiveness, which also implies a more excellent HMT characteristics during the humidification process, shown in the T-h diagram of Fig. 2. It can be seen that the peak water production of the air-heated HDDS rises from m_w=250.84kgh^{-1} to m_w=324.46kgh^{-1} when the minimum enthalpy difference descends from ψ_h=15kJkg^{-1} to ψ_h=5kJkg^{-1}. In reality, after the enthalpy difference alternation, the relevant top humidification effectiveness are ε_h=0.89 at ψ_h=15kJkg^{-1} and ε_h=0.97 at ψ_h=5kJkg^{-1}, respectively. As a result, the humidity difference is enlarged effectively, which contributes to the improvement of the water producing capacity. For the aspect of the thermal efficiency, the top value of GOR is elevated with a magnitude of 35.09%, from *GOR*=2.61 to *GOR*=3.50.

The improvements of the thermodynamic performance will result in the investment growth. In Fig. 8(b), it is observed that the investment growth are mainly attributed to the increase of the HMT areas. According to the simulation results, the relevant area cost is raised from 95.32×10^3¥ at ψ_h=15kJkg^{-1} to 122.75×10^3¥ at ψ_h=5kJkg^{-1}. Thereinto, the cost elevation from the dehumidifier is the largest. As a result of the water production elevation in response to the enthalpy difference alternation, the heat load of the dehumidifier also increase significantly, and then the dehumidifier area grows from A_d=168.50m^2 at ψ_h=15kJkg^{-1} to A_d=221.29m^2 at ψ_h=5kJkg^{-1}. In combination with the properties of the used material of titanium alloy, such cost elevation is prospective. After the accumulation

for all the component cost, the increase magnitude reaches 28.18%, from C_t=97.34×10^3¥ at ψ_h=15kJkg^{-1} to C_t=124.77×10^3¥ at ψ_h=5kJkg^{-1}. Furthermore, due to the consistent trend of the water production and system cost, the final unit cost of water production almost keeps the same after the enthalpy difference variation.

5.5 Effects from the top temperature of the humid air

Besides the performance of the humidification and dehumidification, the air top temperature at the WHRE outlet is also a significant parameter for the desalination performance. Hence, three top temperatures, with 75K, 80K and 85K, are appointed to investigate the corresponding impacts on the thermodynamic and economic performance of the entire HDDS, presented in Fig. 9. Different from the influence from the humidification and dehumidification characteristics, it can be seen a lower top temperature is beneficial for a higher water production, but the influence extent is very limited with a value of Δm_w=6kgh^{-1} at the dehumidification balance conditions. As a matter of fact, the humidity difference will be raised with the increasing top temperature. For instance, the relevant values of the humidity difference are $\Delta\omega$=40.71gkg^{-1} and $\Delta\omega$=53.80gkg^{-1} at T_{a3}=348.15K and 358.15K, respectively. However, the variation law of the air mass flow rate is contrary to that of the absolute humidity reacting to the alternation of the top temperature. During the performance simulation, the terminal temperature difference (TTD) of the WHRE is fixed at TTD_{WHRE}=20K. Hence, the heat load of the WHRE and air mass flow rate are reduced when the top temperature decreases. In combination with the influences from the air humidity difference and mass flow rate, the water production declination with the increasing top temperature is obtained. Furthermore, based on the effect from the heat load of the WHRE to determine the value of GOR, a corresponding elevation from GOR=2.97 at T_{a3}=348.15K to GOR=3.10 at T_{a3}=358.15K is acquired.

At the aspect of the economic performance of the air-heated HDDS, reducing the top temperature will both raise the total cost as well as the UCWP mainly due to a larger heat transfer areas of the dehumidifier at low temperatures. It can be seen that the total cost and UCWP rise to C_t=122.17×10^3¥ and $UCWP$=0.42×10^3¥kg^{-1}h,

when the top temperature arrives at T_{a3}=348.15K.

5.6 Effects from the temperature of the waste heat source

In the current HDDS, the waste heat is applied to heat the air after humidification. It is certain that the temperature of the waste heat source, $T_{e,i}$, is important for the performance of the HDDS. As a result, the thermodynamic and economic performance of the air-heated HDDS at different temperatures of the waste heat are calculated and presented in Fig. 10. It is obvious that a higher temperature of the heat source is significant to raise the water production during dehumidification, from m_w=243.44kgh^{-1} at $T_{e,i}$=393.15K to m_w=341.55kgh^{-1} at $T_{e,i}$=413.15K. Such elevation of the water production is mainly attributed to the increase of the cycling air mass flow rate involved in the system. Actually, at the assumption for the top air temperature, T_{a3}=353.15K, and terminal temperature difference of the waste heat recovery exchanger, TTD_{WHRE}=20K, the mass flow rate of the cycling air rises significantly, from m_{da}=1.41kgs^{-1} at $T_{e,i}$=393.15K to m_{da}=1.98kgs^{-1} at $T_{e,i}$=413.15K at the balance condition of the dehumidifier, while the relevant difference of the humidity ratio before and after dehumidification almost keeps the same under the same temperature variation of the waste heat source. Based on the expression of the water production, an peak elevation amplitude, 40.30%, for the water production is obtained. However, the energy input into the HDDS, mainly referring to the heat load of the WHRE, also increases following the temperature elevation of the waste heat source. Taking the balance condition of the dehumidifier for instance, the corresponding heat load of the WHRE ascends from Q_{WHRE}=49.91kW at $T_{e,i}$=393.15K to Q_{WHRE}=70.03kW at $T_{e,i}$=413.15K. Finally, the GOR is decreased slightly from GOR=3.10 to GOR=2.97.

In response to the alternation of the thermodynamic performance, the variations of the economic aspect also appear. A higher temperature of the waste heat source means a larger areas of the heat exchangers, especially for the surface dehumidifier, which is raised from A_d=170.11m^2 at $T_{e,i}$=393.15K to A_d=238.31m^2 at $T_{e,i}$=413.15K at the balance condition of the dehumidifier. As a result, the relevant total investment rises from C_t=97.82×10^3¥ to

C_t=134.11×10^3¥. Similar with the trend of the GOR with the mass flow rate ratio, it is also obtained that the UCWP almost keeps the same due to the completely reverse variation tendency of the investment and water production.

6. Conclusions

In this paper, the air-heated HDDS, driven by waste heat, is focused. With the modified definition of effectiveness for the humidification and fixed effectiveness model for the dehumidifier, mathematical models to achieve the performance simulation of the air-heated HDDS are established. After the thermodynamic and economic analysis, the following conclusions are given out.

1. At the design conditions, the top water production and GOR reach m_w=289.32kgh^{-1} and 3.06 at the balance conditions of the dehumidifier, respectively. It is found that the total investment of the air-heated HDDS mainly comes from the cost of the dehumidifier area, and the dehumidifier cost arrives at 104.30×10^3¥ while the total investment is 112.55×10^3¥.
2. The thermodynamic and economic performance of the air-heated HDDS is contradictory. The elevation amplitude of the water production, 125.75kgh^{-1}, will contribute to a jump of 379.29×10^3¥ for the total cost of the desalination system when the dehumidification effectiveness rises from 0.8 to 0.9.
3. Reducing the minimum enthalpy difference indicates the elevation of the humidification effectiveness. The elevation both of the water production and total cost is obtained after the declination of the enthalpy difference. However, the final unit cost of water production almost keeps the same.
4. Due to the reverse trend of the humidity difference and air mass flow rate from the variation of the top temperature, the relevant influence on the thermodynamic performance is very limited. Finally, the total cost and UCWP rise to C_t=122.17×10^3¥ and $UCWP$=0.42×10^3¥kg^{-1}h, when the top temperature of the humid air is 348.15K.
5. A higher temperature of the waste heat source indicates both higher water production and total investment

of the air-heated HDDS. The water production of 341.55kgh^{-1} and total investment of 134.11×10^{3}¥ are obtained when the temperature of the water heat arrives at 413.15K. However, the obvious alternation both for the GOR and UCWP are not followed.

Acknowledgements

The authors gratefully acknowledge the financial support by the National Natural Science Foundation of China (Grant No. 51406081), the Hong Kong Scholars Program (Grant No. XJ2017040) and The Hong Kong Polytechnic University.

References

[1] M. Alsehli, J.K. Choi, M. Aljuhan. A novel design for a solar powered multi-stage flash desalination. Solar Energy, 153 (2017): 348-359.

[2] C.H. Qi, H.J. Feng, Q.C. Lv, Y.L. Xing, N. Li. Performance study of a pilot-scale low-temperature multi-effect desalination plant. Applied Energy, 135 (2014): 415-422.

[3] M.M. Germán, D.M. Carvajal, S. Laborie, C. Cabassud, R. Lebrun. Integrated approach in eco-design strategy for small RO desalination plants powered by photovoltaic energy. Desalination, 435 (2018): 246-258.

[4] S. Sadri, R.H. Khoshkhoo, M. Ameri. Optimum exergoeconomic modeling of novel hybrid desalination system (MEDAD+RO). Energy, 149 (2018): 74-83.

[5] H.F. Zheng. Solar Energy Desalination Technology. Amsterdam, Netherlands Elsevier, 2017: 447-535.

[6] M. Capocelli, M. Balsamo, A. Lancia, D. Barba. Process analysis of a novel humidification dehumidification adsorption (HDHA) desalination method. Desalination, 429 (2018): 155-166.

[7] S.A. El-Agouz, S. Ravishankar, M.A. Muthu. Improvement of humidification dehumidification desalination unit using a desiccant wheel. Chemical Engineering Research and Design, 131 (2018): 104-116.

[8] M.H. Hamed, A.E. Kabeel, Z.M. Omara, S.W. Sharshir, Mathematical and experimental investigation of a

409 solar humidification-dehumidification desalinationunit. Desalination, 358 (2015): 9-17.
410 [9] F.A. Al-Sulaiman, M.I. Zubair, M. Atif, P. Gandhidasan, S.A. Al-Dini, M.A. Antar. Humidification
411 dehumidification desalination system using parabolic trough solar air collector. Applied Thermal Engineering,
412 75 (2015): 809-816.
413 [10] E.Z. Mahdizade, M. Ameri. Thermodynamic investigation of a semi-open air, humidification dehumidification
414 desalination system using air and water heaters. Desalination, 482 (2018): 182-198.
415 [11] G. P. Narayan, K.M. Chehayeb, R.K. McGovern, G.P. Thiel, S.M. Zubair, J.H. Lienhard V. Thermodynamic
416 balancing of the humidification dehumidification desalination system by mass extraction and injection.
417 International Journal of Heat and Mass Transfer, 57 (2013): 756-770.
418 [12] K.M. Chehayeb, G.P. Narayan, S.M. Zubair, J.H. Lienhard V. Use of multiple extractions and injections to
419 thermodynamically balance the humidification dehumidification desalination system. International Journal of
420 Heat and Mass Transfer, 68 (2014): 422-434.
421 [13] G.P. Narayan, M.H. Sharqawy, J.H. Lienhard, S.M. Zubair. Thermodynamic analysis of humidification
422 dehumidification desalination cycles. Desalination and Water Treatment, 16 (2010) 339-353.
423 [14] W.F. He, L. Huang, J.R. Xia, W.P. Zhu, X.K. Zhang, Y.K. Wu. Parametric analysis of
424 a humidification dehumidification desalination system using a direct-contact dehumidifier. International
425 Journal of Thermal Sciences, 120 (2017): 31-40.
426 [15] K.M. Chehayeb, G.P. Narayan, S.M. Zubair, J.H. Lienhard V. Thermodynamic balancing of a fixed-size
427 two-stage humidification dehumidification desalination system. Desalination, 369 (2015): 125-139.
428 [16] W. F. He, D. Han, W. P. Zhu, C. Ji. Thermo-economic analysis of a water-heated humidification
429 dehumidification desalination system with waste heat recovery. Energy Conversion and Management, 160
430 (2018): 182-190.

[17] E. Deniz, S. Cinar. Energy, exergy, economic and environmental (4E) analysis of a solar desalination system with humidification-dehumidification. Energy Conversion and Management, 126 (2016): 12-19.

[18] M. I. Zubair, F.A. Al-Sulaiman, M.A. Antar, S.A. Al-Dini, N.I. Ibrahim. Performance and cost assessment of solar driven humidification dehumidification desalination system. Energy Conversion and Management, 132 (2017): 28-39.

[19] M.A. Jamil, S.M. Elmutasim, S.M. Zubair. Exergo-economic analysis of a hybrid humidification dehumidification reverse osmosis (HDH-RO) system operating under different retrofits. Energy Conversion and Management, 158 (2018): 286-297.

[20] D.U. Lawal, S.M. Zubair, M.A. Antar. Exergo-economic analysis of humidification-dehumidification desalination systems driven by heat pump (HP). Desalination, 443 (2018): 11-25.

[21] A. Muley, R.M. Manglik, Experimental study of turbulent flow heat transfer and pressure drop in a plate heat exchanger with chevron plates, Journal of Heat Transfer, 121 (1999):110-117.

[22] M. Mehrgoo, M. Amidpour. Constructal design and optimization of a direct contact humidification dehumidification desalination unit. Desalination, 293 (2012): 69-77.

[23] P. Gandhidasan. Prediction of pressure drop in a packed bed dehumidifier operating with liquid desiccant. Applied Thermal Engineering, 22 (2002): 1117-1127.

[24] M. Sievers, J.H. Lienhard V. Design of flat-plate dehumidifiers for humidification-dehumidification desalination systems. Heat Transfer Engineering, 34 (2013): 543-561.

[25] W.D. Shen, Z.M. Jiang, J.G. Tong, Thermodynamics. Beijing, Higher Education Press, 1982.

[26] G. P. Narayan, J.H. Lienhard, S.M. Zubair. Entropy generation minimization of combined heat and mass transfer devices. International Journal of Thermal Sciences, 49 (2010): 2057-2066.

[27] W.F. He, L.N. Xu, D. Han, L. Gao. Performance analysis of an air-heated humidification dehumidification

desalination plant powered by low grade waste heat. Energy Conversion and Management, 118 (2016): 12-20.

455 [28] **Table 1** Specific dimensions of the plate heat exchangers

δ (mm)	S_p (mm^2)	W(mm)	b (mm)	β(°)	φ
1.5	40460	150	10.3	60	1.3

456 **Table 2** Properties of the involved materials and types of the involved devices

HMTD	Material	Density (kgm^3)	Specific area (m^{2}m^{-3})	Height (m)	Price
Dehumidifier	Titanium Alloy	4507	/	/	260RMBkg^{-1}
WHRE	Stainless Steel	7980	/	/	28RMBkg^{-1}
Packing	Polypropylene	/	250	0.3	2,000RMBm^{-3}

457 **Table 3** Comparison of the dehumidification parameters between the current system and that from Narayan et al.

458 [26]

Term	ε_d	m_{sw}/ m_{da}	T_0 (K)	T_{a3} (K)	RH_2	T_{a1} (K)	m_w (kgh^{-1})	$T_{sw,1}$ (K)
Simulation	0.9	1.5	303.15	363.15	1	307.17	20.16	335.62
Narayan et al. [26]	0.9	1.5	303.15	363.15	1	307.35	21.24	335.94
error(%)	-	-	-		-	0.06	5.1	0.1

459 **Table 4** Design thermal parameters of the air-heated HDDS

S (g/kg)	ψ_h (kJkg^{-1})	ε_d	RH_1	RH_2	T_0 (K)	T_{a3} (K)	TTD_{WHRE} (K)
35	10	0.85	1	1	303.15	353.15	20

460 **Table 5** Thermal parameters of the waste exhaust from a furnace

Term	Unit	Value
$T_{e,i}$	K	403.15
m_e	kg/s	1
x		
CO_2	%	41.2
N_2	%	58.8

461 **Table 6** Information of the seawater pump and blower

Device	Pump			Blower
Power scale (kW)	W_{pu}<0.75	W_{pu}<1.5	W_{pu}<4.0	W_b<2.2
Price (¥)	780	920	1480	1240

462

463 **Fig. 1 Schematic diagram of the air-heated HDDS**

464 **Fig. 2 Heat and mass transfer processes within the air-heated HDDS**

465 **Fig.3 Comparison of the temperature profile during the humidification between the current humidifier and**

466 **that from Chehayeb et al. [12]**

467 **Fig. 4 Strategy and procedures during simulating the thermodynamic and economic performance of the**

468 **air-heated HDDS**

469 **Fig. 5 Performance of the air-heated HDDS at the design conditions**

470 **(a) m_w**

471 **(b) GOR**

472 **Fig. 6 Heat and mass transfer areas and cost of the air-heated HDDS at the design conditions**

473 **(a) Heat transfer areas and packing volume**

474 **(b) Component cost**

475 **Fig. 7 Thermodynamic performance and relevant cost of the air-heated HDDS at different effectiveness of**

476 **the dehumidifier**

477 **(a) m_w and GOR**

478 **(b) Component cost**

479 **(c) Total and UCWP**

480 **Fig. 8 Thermodynamic performance and relevant cost of the air-heated HDDS at different minimum**

481 **enthalpy difference of the humidifier**

482 **(a) m_w and GOR**

483 **(b) Component cost**

484 **(c) Total cost and UCWP**

Fig. 9 Thermodynamic performance and relevant cost of the air-heated HDDS at different top temperatures of the humid air

(a) m_w and GOR

(b) Component cost

(c) Total cost and UCWP

Fig. 10 Thermodynamic performance and relevant cost of the air-heated HDDS at different temperatures of the waste heat source

(a) m_w and GOR

(b) Component cost

(c) Total cost and UCWP

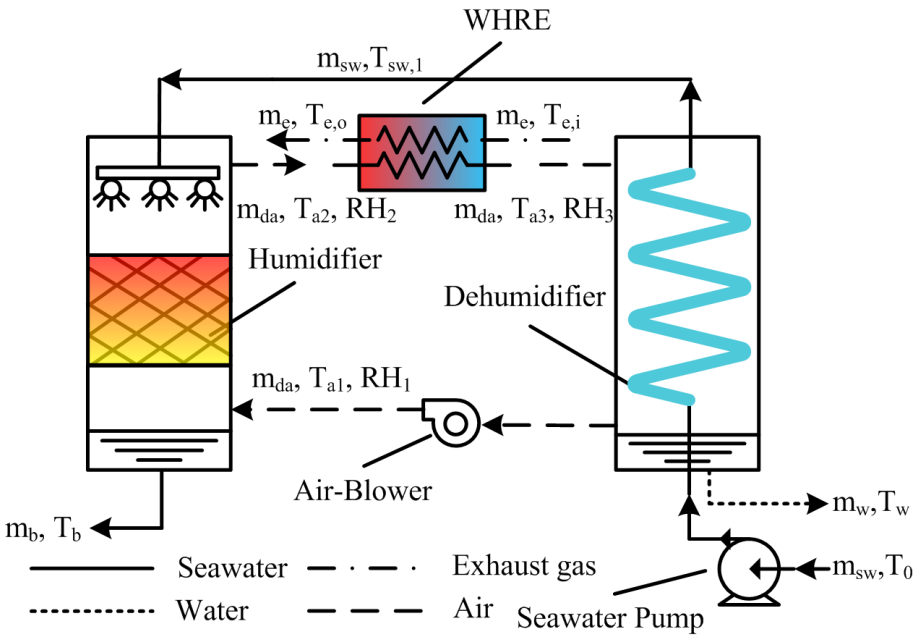

497

498 **Fig. 1** Schematic diagram of the air-heated HDDS

499

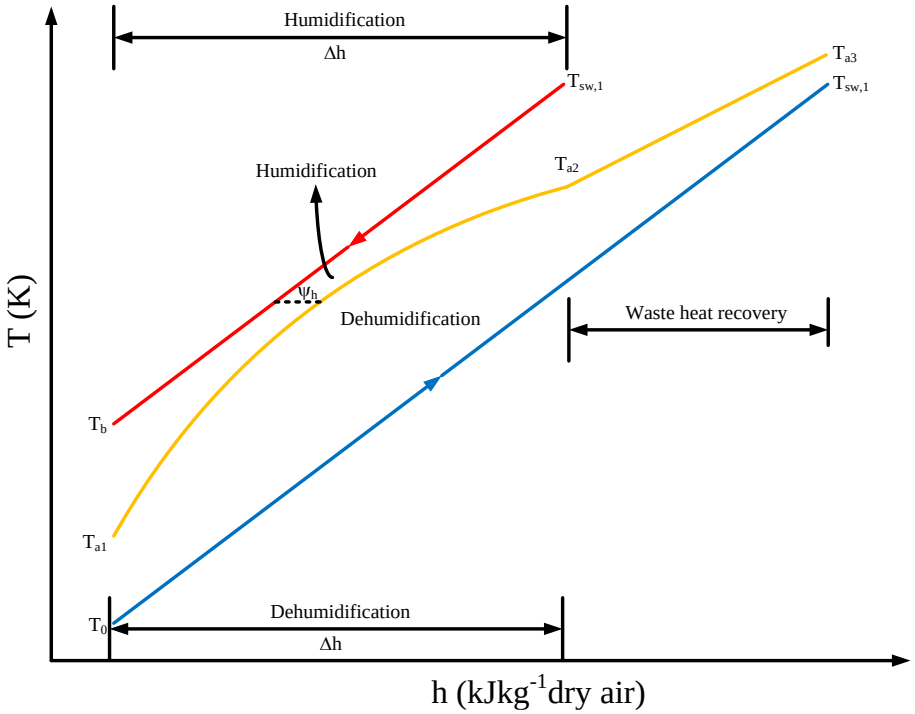

Fig. 2 Heat and mass transfer processes within the air-heated HDDS

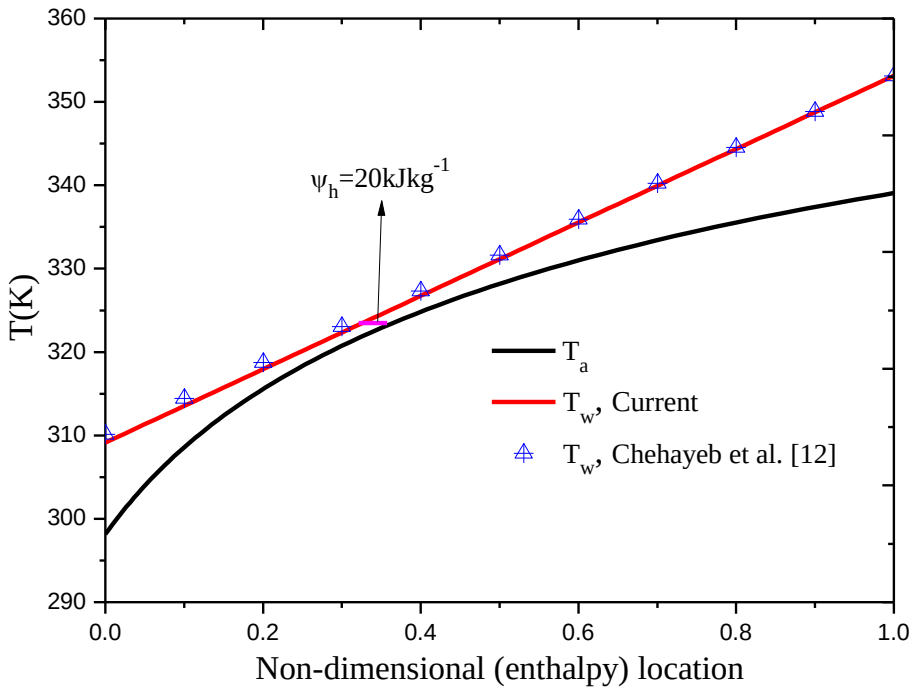

503

504 **Fig. 3** Comparison of the temperature profile during the humidification between the current humidifier and that from Chehayeb et al.

505 [12]

506

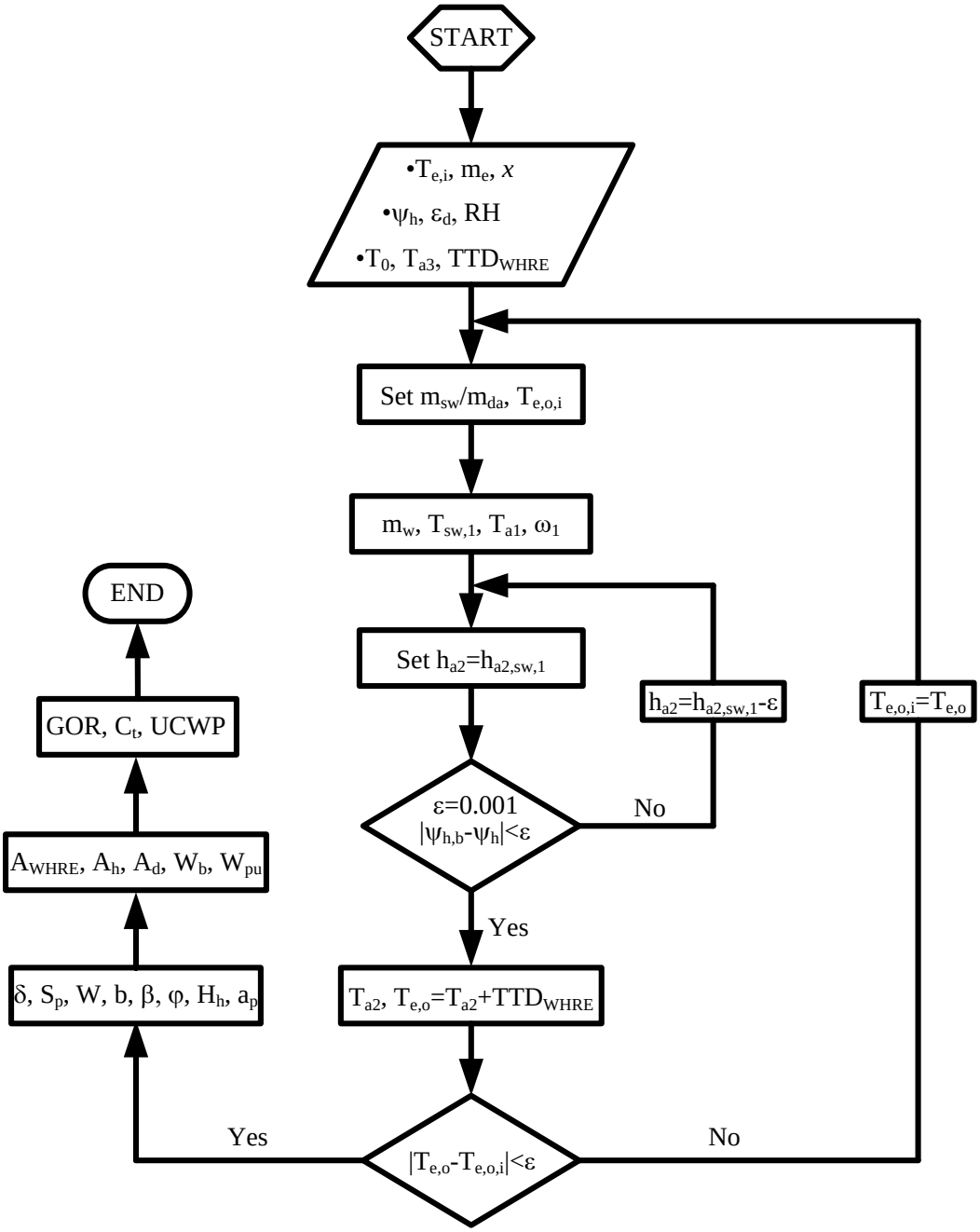

507

508 Fig. 4 Strategy and procedures during simulating the thermodynamic and economic performance of the air-heated HDDS

509

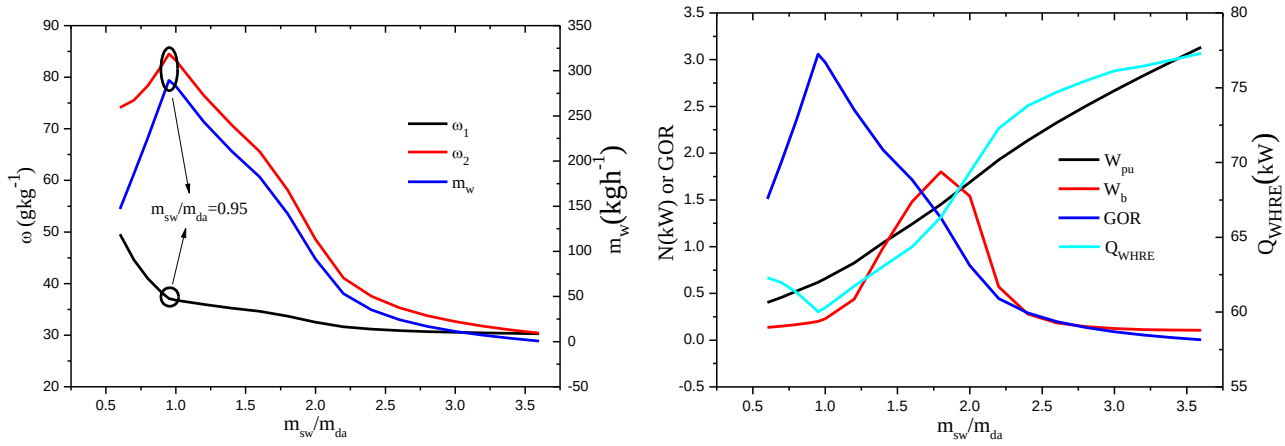

510

511 (a) m_w (b) GOR

512 Fig. 5 Performance of the air-heated HDDS at the design conditions

513

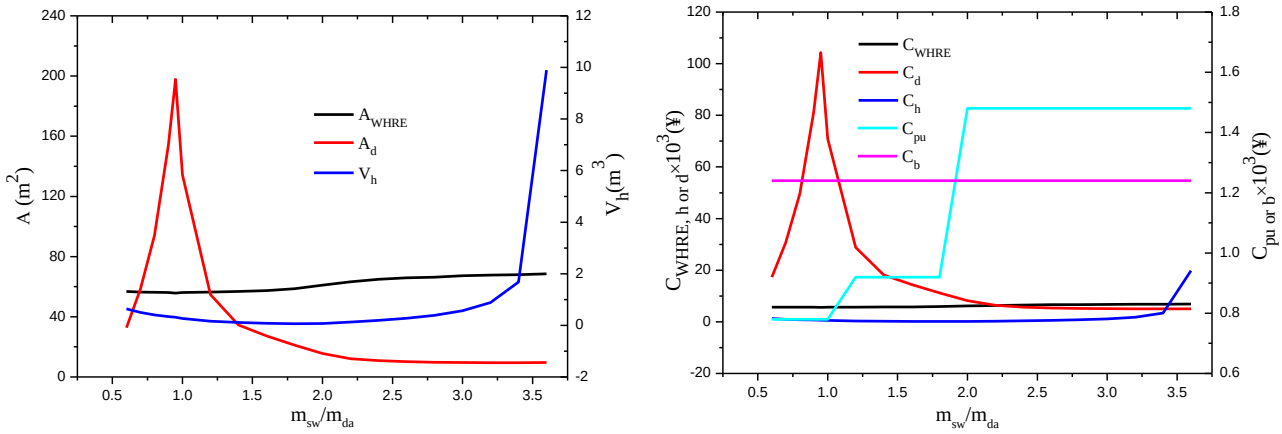

514

515 (a) Heat transfer areas and packing volume (b) Component cost

516 Fig. 6 Heat and mass transfer areas and cost of the air-heated HDDS at design conditions

517

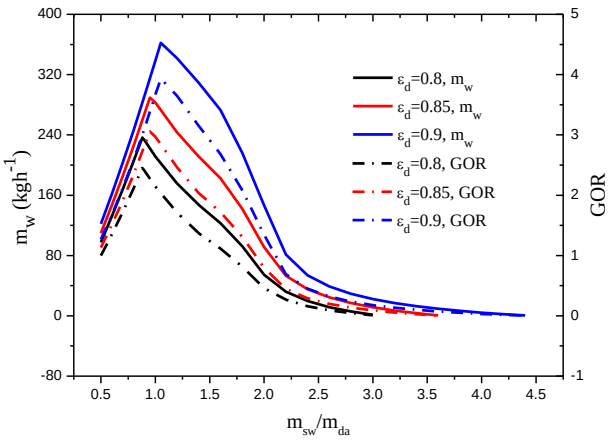

518

519 (a) m_w and GOR

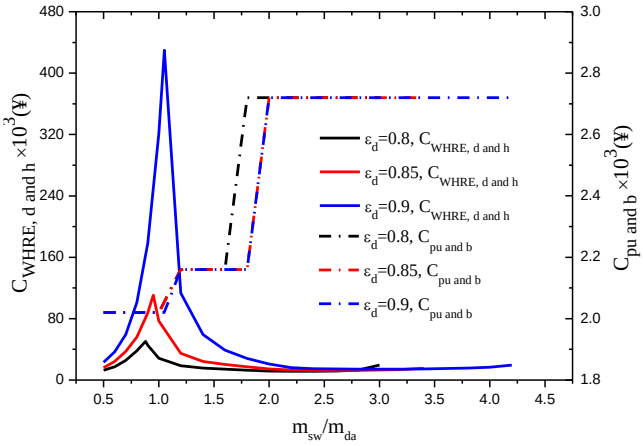

(b) Component cost

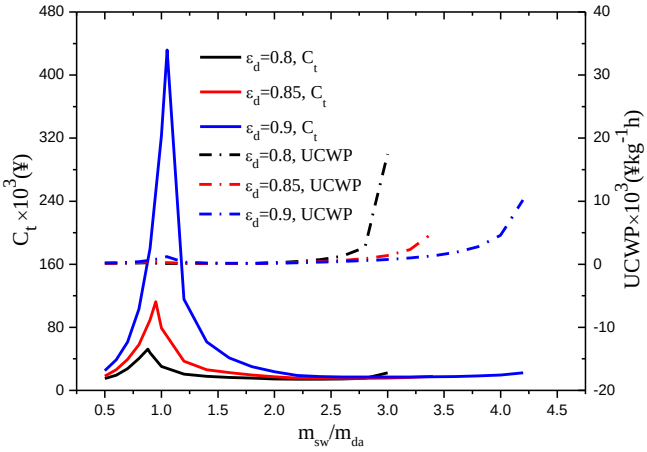

520

521 (c) Total and UCWP

522 Fig. 7 Thermodynamic performance and relevant cost of the air-heated HDDS at different effectiveness of the dehumidifier

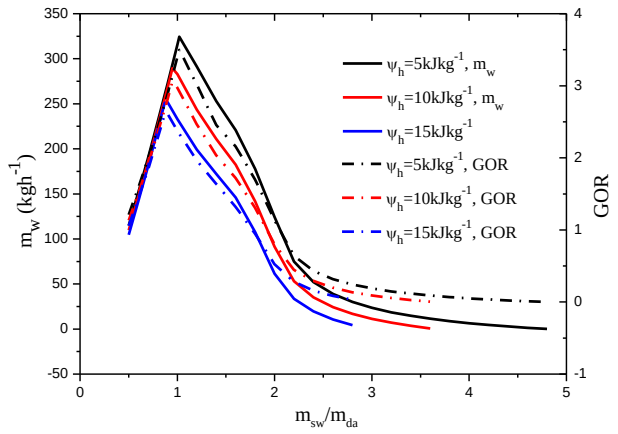

523

524 (a) m_w and GOR

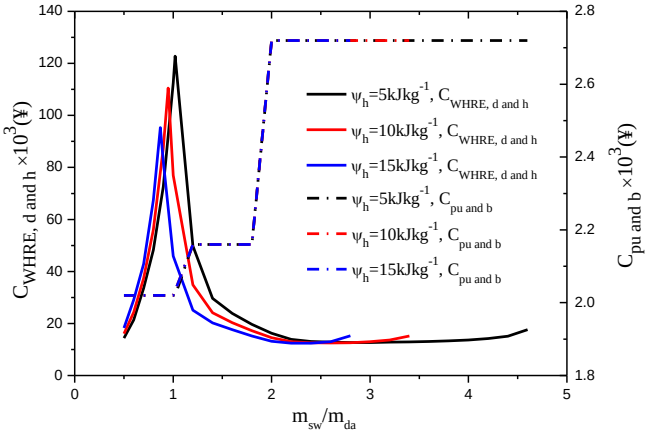

(b) Component cost

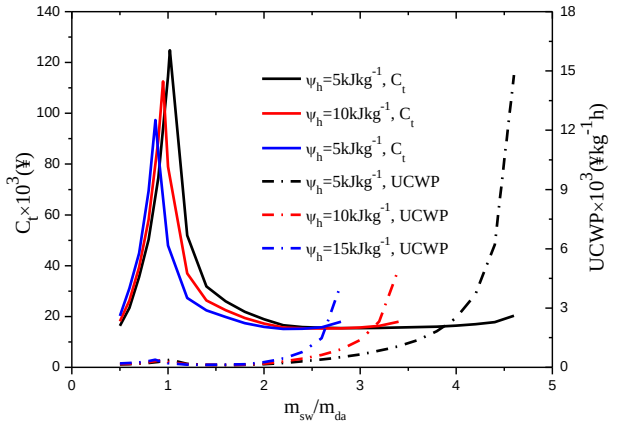

525

526 (c) Total cost and UCWP

527 Fig. 8 Thermodynamic performance and relevant cost of the air-heated HDDS at different minimum enthalpy difference of the

528 humidifier

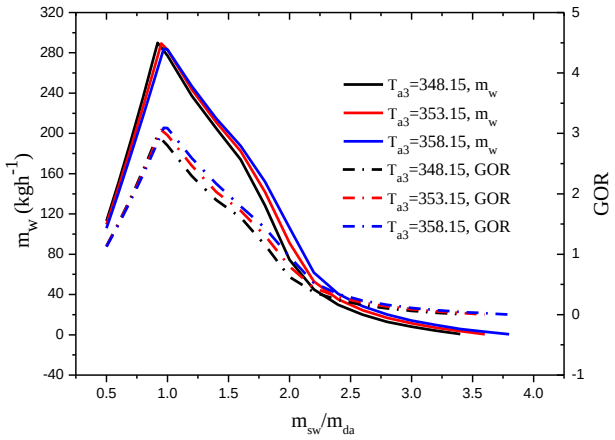

529

530 (a) m_w and GOR

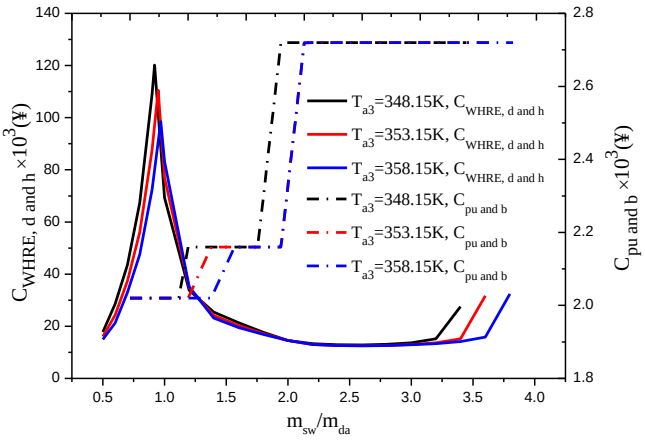

(b) Component cost

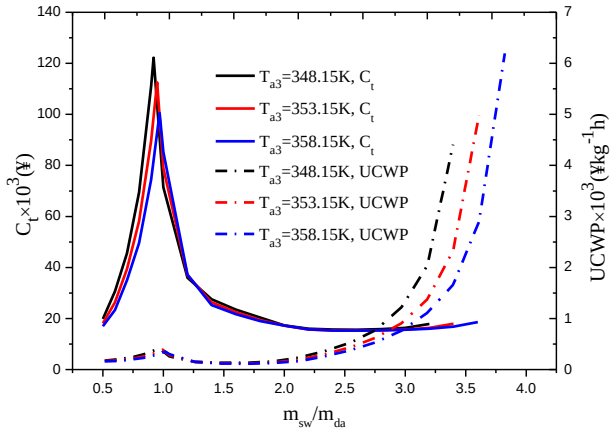

531

532 (c) Total cost and UCWP

533 Fig. 9 Thermodynamic performance and relevant cost of the air-heated HDDS at different top temperatures of the humid air

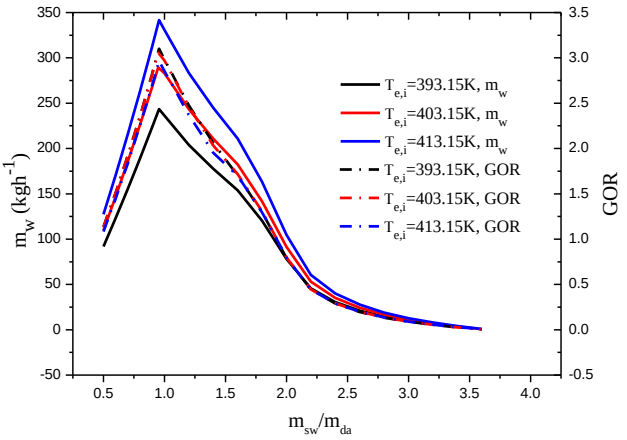

534

535 (a) m_w and GOR

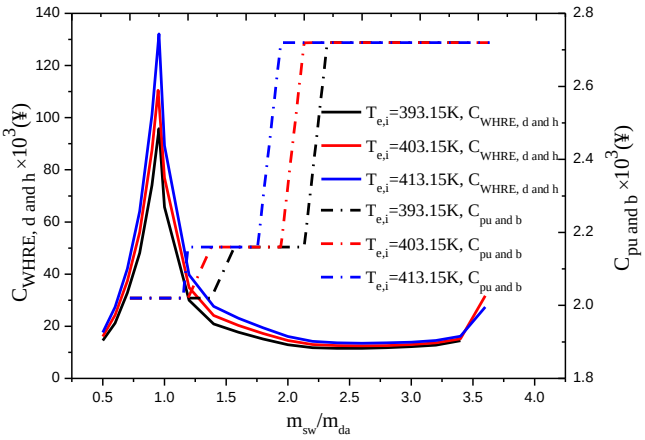

(b) Component cost

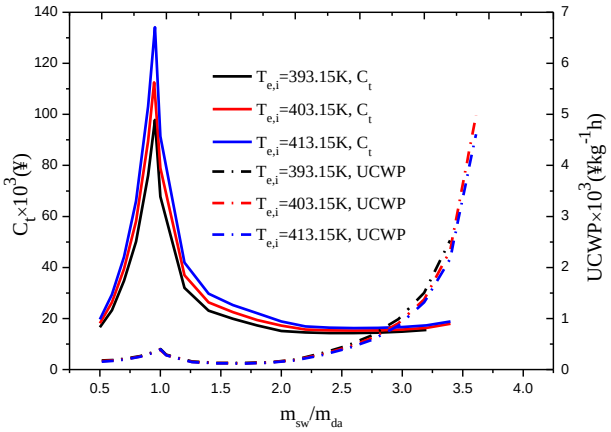

536

537 (c) Total cost and UCWP

538 Fig. 10 Thermodynamic performance and relevant cost of the air-heated HDDS at different temperatures of the waste heat source

539